ARTICLE

Solution-based Synthesis of NiSb Nanoparticles for Electrochemical Activity in Hydrogen Evolution Reaction

Yin-yin Qian†, Jing Yang†, Huan-ran Li, Shi-qi Xing, Qing Yang*

Hefei National Laboratory of Physical Sciences at the Microscale, Department of Chemistry and Laboratory of Nanomaterials for Energy Conversion, University of Science and Technology of China, Hefei 230026, China

(Dated: Received on May 22, 2018; Accepted on June 12, 2018)

A cost-effective, facile solution-based hot-injection synthetic route has been developed to synthesize NiSb nanoparticles in oleylamine (OAm) using commercially available inexpensive precursor with reducing toxicity at a relatively low temperature of 160 °C. Especially, an organic reductant of borane-tert-butylamine complex is intentionally involved in the reaction system to promote a fast reduction of metallic Ni and Sb for the formation of the NiSb nanoparticles. Structural characterizations reveal that the NiSb nanoparticles are hexagonal phase with space group $P6_3/mmc$ and they are composed of small granules with size about 10 nm that tend to form agglomerates with porous-like geometries. This is the first report on the generation of transition metal antimonide via solution-based strategy, and the as-fabricated nanoparticles possess actively electrocatalytic hydrogen evolution reaction (HER) property in acidic electrolytes when the long-chain ligand of OAm adhered on the surface of the nanoparticles is exchanged by ligand-removal and exchange procedure. It is found that the NiSb nanoparticles as a new kind of non-noble-metal HER electrocatalysts only require overpotentials of 437 and 531 mV to achieve high current densities of 10 and 50 mA/cm^2 respectively, as well as exhibit low charge transfer resistance and excellent HER stability.

Key words: Hot-injection synthetic route, NiSb nanoparticles, Ligand-removal and exchange, Hydrogen evolution reaction activity

I. INTRODUCTION

With the ever-increasing global energy requirements and environmental crisis, molecular hydrogen (H_2) has been expected as a desirable energy carrier compared to the traditional fossil fuel due to its highest energy density per unit mass and the only byproduct of water [1, 2]. Among several ways to produce large-scale hydrogen, electrochemical water splitting is considered as the most cost-effective method [3, 4], however, it requires high-activity electrocatalysts to improve the hydrogen evolution reaction (HER) performance [5–7]. Until now, Pt-based electrocatalysts still show the highest activity for HER while the high cost and scarcity of Pt is the biggest obstacles for its practical applications widespreadly [8, 9]. In this regard, there is a great tendency to explore earth-abundant and efficient HER electrocatalysts as promising alternatives to the noble metal-based catalysts. Because that the abundance of Sb in the Earth's crust is about 0.5 parts per million [10], transition metal antimonides are considered to be a new kind of promising electrocatalysts for HER.

Currently, transition metal antimonides have been demonstrated with diverse properties that can be utilized in a wide range of applications, including high-speed optoelectronic devices, infrared detectors, thermoelectric materials, electrocatalysis, and electrode materials for Li/Na ion batteries [11–16]. During the past few years, several research groups have focused on the controlled synthesis of transition metal antimonide nanomaterials with desired chemical and physical properties. However, most of the transition metal antimonide nanomaterials have been prepared by traditional synthesis techniques such as mechanical alloying, chemical alloying, and metal catalyzed vapor-liquid-solid (VLS) growth, which may need high temperature and long reaction time [17–19]. Due to Sb with low surface energy and low solubility [19, 20], it can easily diffuse onto the surface of the nanomaterials to reduce the surface energy, which makes the uniformity and morphology of the materials difficult to control. What's more, as for the fabrication of transition metal antimonide nanomaterials via a hydrothermal/solvothermal process, there are almost not any effective surfactants which are demonstrated to inhibit the agglomeration of the nanoparticles according to previous work [21, 22]. Herein, we present a cost-effective solution-based hot-

†These authors contributed equally to this work.
*Author to whom correspondence should be addressed. E-mail: qyoung@ustc.edu.cn

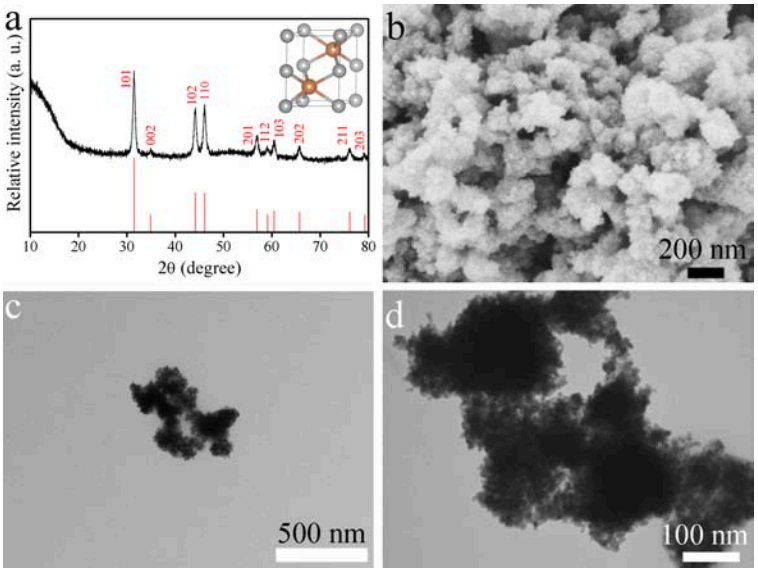

FIG. 1 (a) XRD pattern of the as-synthesized NiSb nanoparticles along with the corresponding standard pattern of hexagonal NiSb (JCPDS card No.03-065-4339), and the inset is schematic representation of the NiSb crystal structure, (b) SEM image, (c) low- and (d) high-magnification TEM images for the NiSb nanoparticles.

injection route to prepare nanostructured NiSb of a typical transition metal antimonide using commercially available precursors at a relatively low temperature of about 160 °C. In detail, the NiSb nanoparticles were fabricated in oleylamine (OAm) from reaction of $Ni(acac)_2{\cdot}xH_2O$ and $Sb(Ph)_3$ with the assistance of strong reductant of borane-tert-butylamine complex, by adaptation of our recently reported methods to InSb nanowires [23]. With the regard of potential applications in HER electrocatalysts of the as-synthesized NiSb nanoparticles, the long-chain surfactant can be exchanged by ligand-removal and exchange procedure. As expected, the NiSb nanoparticles exhibit excellent electrocatalytic performance for HER with super durability and a high cathodic current density of 50 mA/cm^2 when overpotential was at the value of 531 mV. Meanwhile, the solution-based synthetic strategy will be a good prospect of extending the controllable synthesis of other transition metal antimonides.

II. EXPERIMENTS

A. Materials

$Ni(acac)_2{\cdot}xH_2O$, $Sb(Ph)_3$, oleylamine (OAm, 70%), Nafion solution (5 wt%) and borane-tert-butylamine complex (BTB, purity: 97%) were purchased from Alfa Aesar, TCI, and Sigma-Aldrich, respectively. Potassium sulfide anhydrous (K_2S), formamide, hexane and absolute ethanol were purchased from Sinopharm Chemical Reagent Ltd. All reagents and solvents were used as received without any further treatment and purification in the synthesis.

B. Synthesis of NiSb nanoparticles

The fabrication of NiSb nanoparticles was carried out by the method in Ref.[23] with some modifications. In brief, 0.1 mmol of $Ni(acac)_2{\cdot}xH_2O$, 0.1 mmol of $Sb(Ph)_3$ and 5.0 mL of OAm were transferred into a 100 mL three-neck round-bottom flask. After degas at about 110 °C for 20 min under argon flow, the mixture was heated to 160 °C with an addition of reductant of borane tert-butylamine complex in oleylamine. The reaction mixture was kept at 160 °C for 30 min to grow the NiSb nanoparticles. Finally, the product was washed using absolute ethanol and collected for further determination and investigation.

The synthetic route was applied for the synthesis of CoSb and Ag_3Sb similarly, as described in detail in supplementary materials. Meanwhile, the methods on structure characterization in addition to the electrochemical measurements of the as-prepared samples are also provided in supplementary materials.

III. RESULTS AND DISCUSSION

FIG. 1(a) shows a typical XRD pattern of the as-prepared NiSb nanoparticles obtained at approximately 160 °C for 30 min, all the peaks of the sample can be accurately indexed to a pure-phase of hexagonal NiSb. The peaks at 2θ of 31.47°, 34.96°, 44.24°, 46.08°, 56.95°, 59.11°, 60.44°, 65.79°, 76.07°, and 79.31° are in good agreement with (101), (002), (102), (110), (201), (112), (103), (202), (211) and (203) planes of the hexagonal NiSb with space group $P6_3/mmc$ (JCPDS card, No.03-065-4339), and the schematic crystal structure of

DOI:10.1063/1674-0068/cjcp1805113

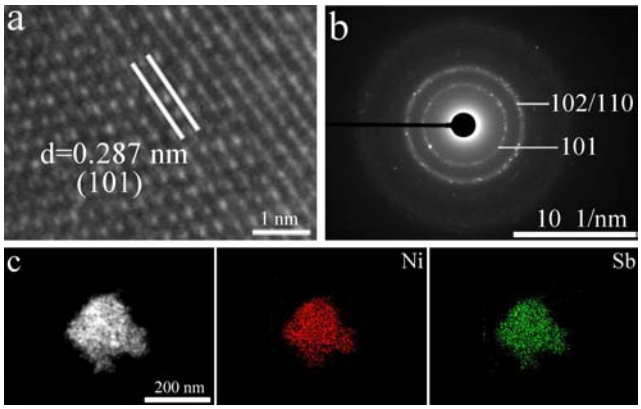

FIG. 2 (a) HRTEM image of the NiSb nanoparticles, (b) SAED pattern and (c) HAADF-STEM image, STEM-EDX elemental mappings of Ni and Sb.

the hexagonal NiSb is displayed in the inset of FIG. 1(a). FIG. 1(b) is a typical SEM image for the hexagonal NiSb nanoparticles that are consisted of small granules with size of about 10 nm in diameter. Seemingly, the nanoparticles connect each other to form agglomerates with porous-like geometries. The morphology observed from TEM images (FIG. 1 (c) and (d)) reveals the same result as the aboved SEM images (FIG. 1(b)).

A high-resolution TEM (HRTEM) image further reveals the microscopic structure of the as-prepared NiSb nanoparticles. Well-resolved lattice fringes are observed in FIG. 2(a), indicating that the NiSb nanoparticles have high crystallinity. The interplanar distance of 0.287 nm agrees well with the (101) plane of the hexagonal NiSb. As shown in FIG. 2(b), the distinct ring patterns in SAED pattern reveal the polycrystalline nature of the NiSb nanoparticles, which are in agreement with the (101), (102), and (110) lattice planes of the hexagonal NiSb nanocrystals. Meanwhile, the HAADF-STEM image and corresponding STEM-EDX elemental mappings are displayed in FIG. 2(c), which confirms the homogeneous distribution with two elements of Ni and Sb in the as-synthesized NiSb nanoparticles. The molar ratio of Ni:Sb is 53.75:46.25 (FIG. S1 in supplementary materials), which is consistent well with the stoichiometric composition of NiSb with 1:1. The synthetic route can also be expanded to prepare other binary transition metal antimonides, such as CoSb and Ag_3Sb (FIG. S2 and S3 in supplementary materials).

The surface of the NiSb nanoparticles synthesized in our present solution-based route is capped with a layer of long-chain OAm ligand which introduces an insulating layer around each nanoparticle. As a result, the highly insulating OAm capping layer limits the charge carrier transport of the as-deposited nanoparticle thin films [24–26], which makes the NiSb nanoparticles unusable as an electrocatalytic material in general. To increase the electrical conductivity and enhance interparticle coupling of the NiSb nanoparticles thin films, we therefore employed an inorganic capping approach in which OAm ligands were replaced by smaller inorganic ions in a phase-transfer process [27]. In detail, we treated the solutions of OAm-capped NiSb nanoparticles in hexane with the solution of S^{2-} in formamide, then the mixture was ultrasonicated for about 20 min leading to an absolute phase transfer of the NiSb nanoparticles from hexane to the formamide phase, and it is found that the phase transfer can be easily observed by the color change in hexane and formamide phases, as shown in FIG. 3(a). The effectiveness of the ligand-removal procedure has been examined by ATR-FTIR spectra. In FIG. 3(b), the bands at 3322 and 1564 cm^{-1} corresponding to N−H stretching and bending modes disappeared after the exchange of OAm ligand with S^{2-} [28, 29], suggesting the complete removal of the OAm ligand in the ligand-removal and exchange procedure. The bands at 2800−3000 cm^{-1} in the ATR-FTIR spectra corresponding to C−H stretching modes could be assigned to the unevaporated hexane [30]. The chemical states of the as-prepared NiSb nanoparticles were investigated by XPS spectra. As shown in FIG. 3(c), the Ni 2p spectrum exhibits two peaks, $2p_{1/2}$ and $2p_{3/2}$, located at 873.4 and 855.4 eV, respectively, as well as two shake-up satellite peaks (shorted as Sat.) centered at 879.9 and 861.2 eV [31, 32], confirming the existence of Ni(II) or Ni(III) states in the sample. Two other peaks (labeled with *) located at 869.7 and 852.6 eV were likely due to the zero valence Ni in NiSb [33]. In the Sb 3d XPS spectrum (FIG. 3(d)), the peaks at 537.2 and 527.8 eV also suggest the existence of zero valence Sb in NiSb [34, 35]. In addition, two peaks located at 539.5 and 530.2 eV confirm the presence of Sb(III) state, which is probably due to somewhat surface oxidation [34]. The above-mentioned detection was further comfirmed by the fitted XPS data (FIG. S4 in supplementary materials).

The HER performance of the as-synthesized NiSb nanoparticles deposited on a carbon cloth (CC) electrode was examined in 0.5 mol/L H_2SO_4 aqueous electrolyte using a typical three-electrode setup at room temperature. All the potentials in this work were calibrated to the reversible hydrogen electrode (RHE) [36, 37]:

$$E_{\mathrm{RHE}} = E_{\mathrm{Ag/AgCl}} + 0.059 \times \mathrm{pH} + 0.197 \qquad (1)$$

As shown in FIG. 4(a), the polarization curve of the NiSb nanoparticles exhibits an onset potential of 290 mV. To achieve the current densities of 10 mA/cm^2 and as high as 50 mA/cm^2, small overpotentials of 437 and 531 mV are required, respectively. In addition, the current density (j) increases rapidly at more negative potentials, which corresponds to highly catalytic H_2 evolution. To probe the durability of the NiSb nanoparticles electrocatalyst, we cycled the NiSb catalyst continuously for 500 cycles at a scan rate of 50 mV/s in 0.5 mol/L H_2SO_4 (FIG. 4(a)), the obtained polariza-

DOI:10.1063/1674-0068/cjcp1805113

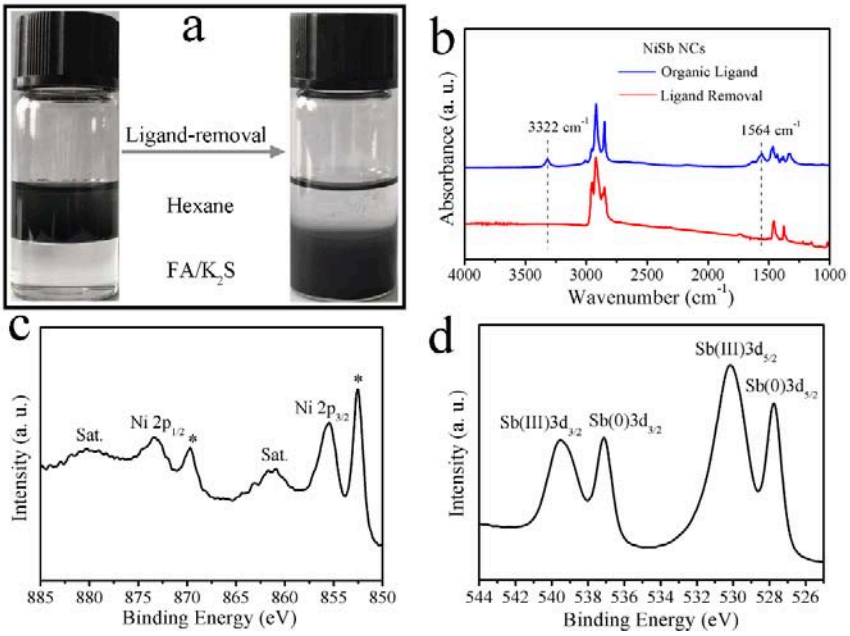

FIG. 3 (a) Photographs illustrating phase transfer of NiSb nanoparticles from hexane to formamide, (b) ATR-FTIR spectra of the as-obtained NiSb nanoparticles, blue and red curves refer to the results of the sample before and after phase transfer, (c) XPS spectrum of Ni 2p, and (d) XPS spectrum of Sb 3d in NiSb nanoparticles.

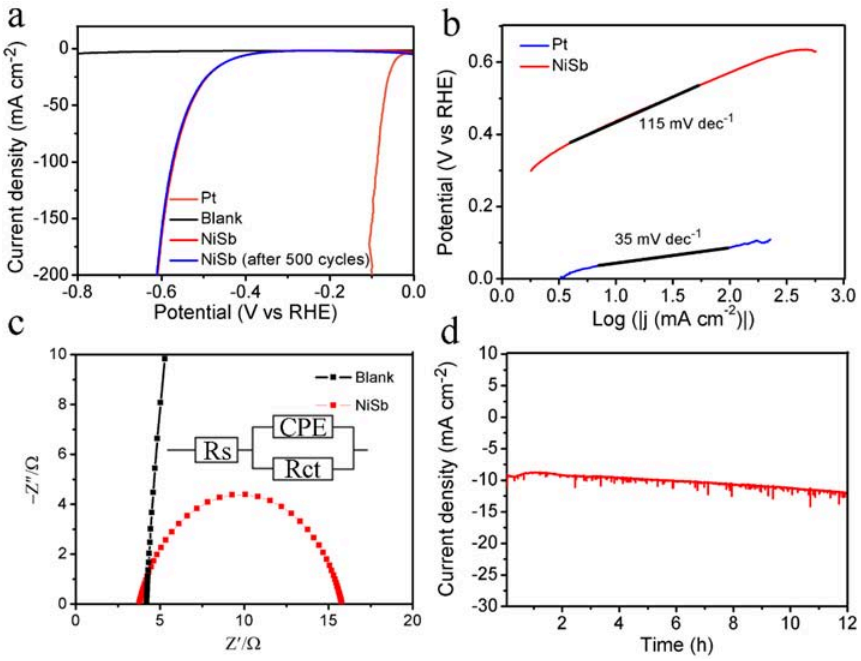

FIG. 4 (a) Polarization curves and (b) Tafel slopes of the as-prepared NiSb nanoparticles electrocatalyst, (c) EIS at the overpetential of 700 mV, and (d) time-dependent current density curve of the as-prepared NiSb nanoparticles electrocatalyst.

tion curve remains similar to the initial one, indicating high durability under HER conditions. In order to investigate the kinetics of the NiSb nanoparticles during the HER process, the Tafel slopes were determined by fitting the linear portions of the Tafel plots to the Tafel equation:

$$\eta = b \log j + a \tag{2}$$

where η represents the applied overpotential, j represents the current density, b is the Tafel slope and a

DOI:10.1063/1674-0068/cjcp1805113

is the intercept relative to the exchange current density. In FIG. 4(b), the observed Tafel slope of approximately 115 mV/dec for the NiSb nanoparticles indicates that the HER takes place through a Volmer-step-determined Volmer-Heyrovsky mechanism [38–42]. To further study the electrocatalytic kinetic process of the NiSb nanoparticles, the electrochemical impedance spectroscopy (EIS) was also performed under HER conditions at overpotential of 700 mV, as depicted in FIG. 4(c). The Nyquist plot of the EIS spectrum of NiSb nanoparticles shows a low charge transfer resistance ($R_{\rm ct}$) of 12.02 Ω, which indicates the electrocatalytic kinetics with a fast reaction rate [43, 44]. The long-term stability of the NiSb nanoparticles electrocatalyst was tested under the overpotential condition of 437 mV (FIG. 4(d)), even after a long period of 12 h, the current density remained almost constant, which suggested that the NiSb catalyst exhibits excellent HER stability [45]. In order to further test the stability of the catalyst, the polarization curves of NiSb nanoparticles before and after 5000 CV (cyclic voltammetry) cycles (more than 2000 cycles) in a 0.5 mol/L H_2SO_4 solution is conducted (FIG. S5 in supplementary materials). After 5000 CV cycles, the negligible difference in the curves also indicates that the NiSb nanoparticles have high stability.

IV. CONCLUSION

We have demonstrated that the pure-phase binary transition metal antimonide NiSb is prepared via a low-temperature solution-based growth strategy, employing $Ni(acac)_2{\cdot}xH_2O$ and $Sb(Ph)_3$ as the precursors. XRD, SEM, TEM, EDS, and XPS examinations confirm the structure, morphology, composition, and elements distribution of the as-prepared NiSb nanoparticles. The highly insulating OAm capping layer adhered on the surface of the NiSb nanoparticles can be exchanged using a ligand-removal and exchange process, which has been examined by ATR-FTIR spectra. The electrocatalytic HER performance of the NiSb nanoparticles has been intensively studied and it is found that the NiSb nanoparticles exhibit good activity and stability in an acidic medium. Our synthetic route can also be expanded to prepare other binary transition metal antimonides, which will be intensively investigated in the coming steps.

Supplementary materials: Additional sample preparation, detailed characterization, electrochemical measurements of the as-prepared samples in FIG. S1−S5 are provided.

V. ACKNOWLEDGEMENTS

This work was supported by the National Natural Science Foundation of China (No.21571166 and No.51271173). The authors are grateful to Professor Shuji Ye at USTC for assisting with experiments of ATR-FTIR detection.

[1] H. Wang, Q. Zhang, H. Yao, Z. Liang, H. W. Lee, P. C. Hsu, G. Zheng, and Y. Cui, Nano Lett. **14**, 7138 (2014).
[2] C. G. Morales-Guio, L. A. Stern, and X. Hu, Chem. Soc. Rev. **43**, 6555 (2014).
[3] Q. Li, N. Mahmood, J. Zhu, Y. Hou, and S. Sun, Nano Today **9**, 668 (2014).
[4] J. Yin, Q. Fan, Y. Li, F. Cheng, P. Zhou, P. Xi, and S. Sun, J. Am. Chem. Soc. **138**, 14546 (2016).
[5] A. J. Bard and M. A. Fox, Acc. Chem. Res. **28**, 141 (1995).
[6] M. Dresselhaus and I. Thomas, Nature **414**, 332 (2001).
[7] M. G. Walter, E. L. Warren, J. R. McKone, S. W. Boettcher, Q. Mi, E. A. Santori, and N. S. Lewis, Chem. Rev. **110**, 6446 (2010).
[8] R. Subbaraman, D. Tripkovic, D. Strmcnik, K. C. Chang, M. Uchimura, A. P. Paulikas, V. Stamenkovic, and N. M. Markovic, Science **334**, 1256 (2011).
[9] B. E. Conway and B. V. Tilak, Electrochim. Acta **47**, 3571 (2002).
[10] L. Liang, Y. Xu, C. Wang, L. Wen, Y. Fang, Y. Mi, M. Zhou, H. Zhao, and Y. Lei, Energy Environ. Sci. **8**, 2954 (2015).
[11] T. Caillat, J. P. Fleurial, and A. Borshchevsky, J. Phys. Chem. Solids **58**, 1119 (1997).
[12] L. Yang, H. H. Hng, D. Li, Q. Y. Yan, J. Ma, T. J. Zhu, X. B. Zhao, and H. Huang, J. Appl. Phys. **106**, 013705 (2009).
[13] P. Ravindran, A. Delin, P. James, B. Johansson, J. M. Wills, R. Ahuja, and O. Eriksson, Phys. Rev. B **59**, 15680 (1999).
[14] M. Wachtler, M. Winter, and J. O. Besenhard, J. Power Sources **105**, 151 (2002).
[15] J. M. Mosby and A. L. Prieto, J. Am. Chem. Soc. **130**, 10656 (2008).
[16] J. X. Zhu, T. Sun, J. S. Chen, W. H. Shi, X. J. Zhang, X. W. Lou, S. Mhaisalkar, H. H. Hng, F. Boey, J. Ma, and Q. Y. Yan, Chem. Mater. **22**, 5333 (2010).
[17] L. M. L. Fransson, J. T. Vaughey, R. Benedek, K. Edstrom, J. O. Thomas, and M. M. Thackeray, Electrochem. Commun. **3**, 317 (2001).
[18] J. T. Vaughey, C. S. Johnson, A. J. Kropf, R. Benedek, M. M. Thackeray, H. Tostmann, T. Sarakonsri, S. Hackney, L. Fransson, K. Edstrom, and J. O. Thomas, J. Powers Sources **97/98**, 194 (2001).
[19] J. Chen, Z. Yin, D. Sim, Y. Y. Tay, H. Zhang, J. Ma, H. H. Hng, and Q. Yan, Nanotechnology **22**, 325602 (2011).
[20] Q. Yan, T. Kim, A. Purkayastha, P. G. Ganesan, M. Shima, and G. Ramanath, Adv. Mater. **17**, 2233 (2005).

DOI:10.1063/1674-0068/cjcp1805113

[21] L. Kumari, W. Li, J. Huang, and P. P. Provencio, J. Phys. Chem. C **114**, 9573 (2010).
[22] C. Li, J. Hu, Q. Peng, and X. Wang, Mater. Chem. Phys. **110**, 106 (2008).
[23] Y. Qian and Q. Yang, Nano Lett. **17**, 7183 (2017).
[24] M. V. Kovalenko, M. Scheele, and D. V. Talapin, Science **324**, 1417 (2009).
[25] M. V. Kovalenko, M. I. Bodnarchuk, J. Zaumseil, J. S. Lee, and D. V. Talapin, J. Am. Chem. Soc. **132**, 10085 (2010).
[26] J. S. Lee, M. V. Kovalenko, J. Huang, D. S. Chung, and D. V. Talapin, Nat. Nanotech. **6**, 348 (2011).
[27] A. Nag, M. V. Kovalenko, J. S. Lee, W. Y. Liu, B. pokoyny, and D. V. Talapin, J. Am. Chem. Soc. **133**, 10612 (2011).
[28] X. Liu, X. L. Wang, B. Zhou, W. C. Law, A. N. Cartwright, and M. T. Swihart, Adv. Funct. Mater. **23**, 1256 (2013).
[29] X. M. Lu, H. Y. Tuan, J. Y. Chen, Z. Y. Li, B. A. Korgel, and Y. N. Xia, J. Am. Chem. Soc. **129**, 1733 (2007).
[30] T. D. Schladt, T. Graf, and W. Tremel, Chem. Mater. **21**, 3183 (2009).
[31] Y. J. Wang, Y. Z. Zhang, J. K. Ou, Q. Zhao, M. Liao, and D. Xiao, RSC Adv. **6**, 547 (2016).
[32] H. S. Hou, M. J. Jing, Y. C. Yang, Y. R. Zhu, L. B. Fang, W. X. Song, C. C. Pan, X. M. Yang, and X. B. Ji, ACS Appl. Mater. Interfaces **6**, 16189 (2014).
[33] S. H. Dong, C. X. Li, and L. W. Yin, Eur. J. Inorg. Chem. **2018**, 992 (2018).
[34] H. S. Hou, X. Y. Cao, Y. C. Yang, L. B. Fang, C. C. Pan, X. M. Yang, W. X. Song, and X. B. Ji, Chem. Commun. **50**, 8201 (2014).
[35] L. Y. Liang, Y. Xu, L. Y. Wen, Y. L. Li, M. Zhou, C. L. Wang, H. P. Zhao, U. Kaiser, and Y. Lei, Nano Res. **10**, 3189 (2017).
[36] J. Yang, C. Wang, H. Ju, Y. Sun, S. Xing, J. Zhu, and Q. Yang, Adv. Funct. Mater. **27**, 1703864 (2017).
[37] C. Wang, T. Ding, Y. Sun, X. Zhou, Y. Liu, and Q. Yang, Nanoscale **7**, 19241 (2015).
[38] B. E. Conway and B. V. Tilak, Electrochim. Acta **47**, 3571 (2002).
[39] S. Marini, P. Salvi, P. Nelli, R. Pesenti, M. Villa, M. Berrettoni, G. Zangari, and Y. Kiros, Electrochim. Acta **82**, 384 (2012).
[40] Y. Pan, Y. R. Liu, J. C. Zhao, K. Yang, J. L. Liang, D. D. Liu, W. H. Hu, D. P. Liu, Y. Q. Liu, and C. G. Liu, J. Mater. Chem. A **3**, 1656 (2015).
[41] X. Zhou, J. Jiang, T. Ding, J. Zhang, B. Pan, J. Zuo, and Q. Yang, Nanoscale **6**, 11046 (2014).
[42] Y. Liu, X. Zhou, T. Ding, C. Wang, and Q. Yang, Nanoscale **7**, 18004 (2015).
[43] E. J. Popczun, C. G. Read, C. W. Roske, N. S. Lewis, and R. E. Schaak, Angew. Chem. Int. Ed. **53**, 5427 (2014).
[44] D. Voiry, J. Yang, and M. Chhowalla, Adv. Mater. **28**, 6197 (2016).
[45] Y. Yang, Z. Lun, G. Xia, F. Zheng, M. He, and Q. Chen, Energy Environ. Sci. **8**, 3563 (2015)

DOI:10.1063/1674-0068/cjcp1805113